Propeller performance in presence of freestream: applications in modeling multirotor UAVs

Mojtaba Hedayatpour[1], Mehran Mehrandezh[1], and Farrokh Janabi-Sharifi[2]

[1] Faculty of Engineering and Applied Science, University of Regina, Regina SK S4S 0A2, Canada,
{hedayatm,mehran.mehrandezh}@uregina.ca,
[2] Department of Mechanical & Industrial Engineering, Ryerson University, Toronto ON M5B 2K3, Canada
fsharifi@ryerson.ca

Abstract. This chapter presents mathematical modeling for thrust force and moments generated by a propeller in presence of freestream. In particular, the effects of a uniform freestream on propeller's performance are investigated. We introduce some of the applications of the proposed model in the design of multi-rotor UAVs which helps to increase stability or maneuverability of the vehicle. In the end, simulation results for thrust force and moments of an example propeller in presence of a uniform freestream are presented.

Keywords: propeller, freestream, unmanned aerial vehicle, mathematical modeling, spinning UAVs

1 Introduction

Multi-rotors have gained significant attention in recent years. Due to their simplicity and maneuverability, they have been used in a broad spectrum of applications such as bio-engineering [1], agronomy [2] , calibrating antenna of a telescope [3] and inspection of infrastructures [4].

A special type of multi-rotors with four rotors, known as quadcopters, has been extensively studied and there is a vast literature about their modeling, design, control and path planning. These vehicles normally have an even number of propellers half of which turn in the opposite direction of the remaining propellers. Modeling and full control of a quadcopter can be found in [5]. Quadcopters with fixed rotors fall under the under-actuated and non-holonomic flying machine categories. In the past decades, many different control strategies have been developed to deal with their under-actuation to improve their performance, agility and stability [6], [7].

Recently, there have been considerable attempts on designing simpler flying vehicles with the minimum number of actuators. A type of these highly under-actuated flying vehicles is called spinning UAV, also known as spinners. They typically fly while spinning with a high angular velocity and they are controllable in three translational degrees of freedom [8].

In modeling of UAVs, aerodynamic model of propellers plays an important role as it determines the majority of forces and moments in the system. Therefore, an accurate model for the propellers is crucial in analyzing such a system. In the literature, typically, the thrust force and moments generated by the propeller is assumed to be proportional to the square of its angular velocity and the effects of freestream on its performance is usually neglected by assuming small freestream velocities [9], [10], [11]. However, this model is not valid in high speed flight and its accuracy deteriorates as flight speed increases [12], [8].

It is also known that the freestream may affect propeller's performance depending on its direction and magnitude. Generally, these effects could change propeller's performance in two ways: i) changing the effective angle of attack of the blades; and ii) changing the local airflow velocity over the blades. The former effect is caused when there is a freestream with its velocity vector parallel to the angular velocity vector of the propeller while the latter is caused by any freestream with its velocity vector perpendicular to that of the propeller. Studying these effects not only helps us to derive a more realistic mathematical model for multi-rotors but also helps to find more stable and power-optimal configurations for such vehicles [12]. Here, we use Blade Element Theory (BET) to calculate the thrust force and moment of each blade element.

This chapter presents mathematical modeling for multi-rotor UAVs by taking into account the effects of freestream. We begin with presenting a mathematical model of thrust force and moments of a propeller in presence of freestream, this proposed propeller model is used to derive equations of motion of a quadcopter with angled thrust vectors as well as equations of motion of a spinning UAV with two rotors and a streamline-shape fuselage.

For the quadcopter with angled thrust vector, by utilizing the proposed propeller model and according to [12], more stable/maneuverable configurations can be found. For the spinners, due to the fast rotational motion, the freestream changes the thrust force and moments generated by the propeller significantly. Therefore, taking the effects of freestream into account is crucial in modeling and control of spinners. We address this issue by incorporating the effects of freestream on propeller's performance into mathematical modeling of spinners. The proposed models in this chapter can be used for studying controller performance in more details or can be used in designing a more accurate simulator for multi-rotor UAVs.

Notation: Throughout the chapter, matrices are represented by straight boldface letters and all vectors are represented by italicized boldface letters. For example, rotation matrix from frame i to frame j is represented by ${}^{j}\mathbf{R}_{i}$. In addition, the term ${}^{I}\boldsymbol{\omega}_{p}$ denotes $\boldsymbol{\omega}$ belongs to p and is expressed in frame I. Angular velocity vector of the vehicle is represented by $\boldsymbol{\omega}_B = (p, q, r)^T$ where p, q and r are roll, pitch and yaw rates respectively. Also, 2-Norm of $\boldsymbol{\omega}$ is represented by $\|\boldsymbol{\omega}\|$ and absolute value of scalar s is shown by $|s|$.

2 Propeller Model in Presence of Freestream

Suppose we have a propeller turning with angular velocity $\boldsymbol{\omega}_p$ as expressed in a frame attached to the center of the rotor as shown in Fig. 1. The propeller has two blades of radius R_b and is assumed to have constant chord c. For simplicity, first, we assume there is a uniform freestream with velocity vector $\boldsymbol{V}_{\infty_1}$, as shown in blue in Fig. 1, which is parallel to the y-axis. Later, to generalize the model for any freestream with an arbitrary velocity vector, we will continue our analysis by assuming a freestream with its velocity vector parallel to that of the propeller.

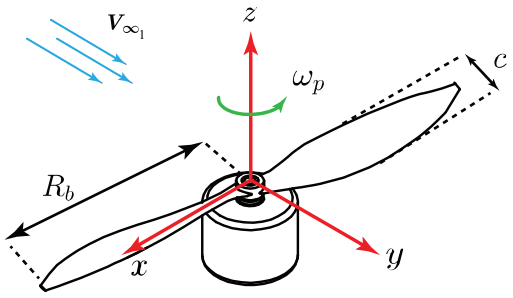

Fig. 1. Schematic of a propeller with a frame attached to its COM.

Consider a blade element (small hashed area in Fig. 2) of length c and differential width dr_b where r_b is the distance of the blade element from the root of the blade. As shown in Fig. 2, the rotation of the blade generates relative air flow velocity of magnitude $r_b\|\boldsymbol{\omega}_p\|$, over each blade element. As the propeller is turning, the relative air flow velocity over the blade element could either be increased or decreased depending on the azimuth angle of the blade and direction of the freestream velocity. The azimuth angle ψ_p is defined as the angle between the blade and the direction of $\boldsymbol{V}_{\infty_1}$. Therefore, the resultant relative air flow velocity over each blade element can be written as:

$$v = r_b\|\boldsymbol{\omega}_p\| + \|\boldsymbol{V}_{\infty_1}\| \sin\psi_p \tag{1}$$

In Fig. 2, for the advancing blade ($0 \leq \psi_p \leq \pi$), freestream velocity increases the relative air flow velocity over the blade and for the retreating blade ($\pi \leq \psi_p \leq 2\pi$), it decreases the relative air flow velocity. The changes in the relative air flow velocity with azimuth angle affects the overall thrust force of the propeller and it generates a moment in the direction of the freestream velocity as shown in blue. Therefore, using (1) and according to *Blade Element Theory*, thrust force and moments of each blade element can be found as follows:

$$df_p = \frac{1}{2}\rho_a c C_L v^2 dr_b \tag{2}$$

$$d\tau_{d_p} = \frac{1}{2}\rho_a c C_D v^2 r_b dr_b \tag{3}$$

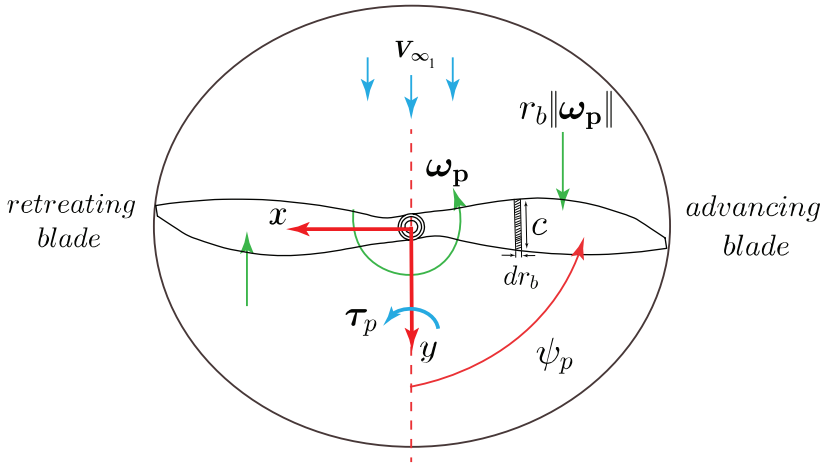

Fig. 2. A propeller in presence of freestream.

$$d\tau_p = \frac{1}{2}\rho_a c C_L v^2 r_b \sin\psi dr_b \tag{4}$$

where ρ_a represents air density and C_L and C_D are the lift and drag coefficients of the airfoil of the blade respectively. Also, f_p represents thrust force of the blade element, τ_{d_p} represents the moment due to drag force of the blade element and τ_p represents the moment due to change in thrust force with respect to the azimuth angle of the blade.

By integrating (2), (3) and (4) over blade radius r_b and azimuth angle ψ_p, average thrust force and the average moments for one blade as functions of freestream velocity and angular velocity of the propeller can be found as follows:

$$f_p = \frac{1}{2}\rho_a c C_L \left(\frac{2R_b^3}{3}\|\boldsymbol{\omega}_p\|^2 + \|\boldsymbol{V}_{\infty_1}\|^2 R_b\right) \tag{5}$$

$$\tau_{d_p} = \frac{1}{4}\rho_a c C_D \left(R_b^4\|\boldsymbol{\omega}_p\|^2 + \|\boldsymbol{V}_{\infty_1}\|^2 R_b^2\right) \tag{6}$$

$$\tau_p = \frac{1}{2}\rho_a c C_L R_b^3 \|\boldsymbol{\omega}_p\|\|\boldsymbol{V}_{\infty_1}\| \tag{7}$$

Note that by assuming zero freestream velocity, equations (5), (6) and (7) yield the simplified model for thrust force and moments of a propeller which is widely used in the literature (i.e., [13], [14], [15], [16]).

Using the proposed model, simulation results for two complete turns of a propeller with angular velocity $\|\boldsymbol{\omega}_p\| = 900$ rad/s in presence of freestream is presented in Fig. 3. Note that the direction of rotation and freestream velocity are the same as those in Fig. 2. The remaining parameters of the simulations are as follows: $c = 0.03$ m, $C_L = 1.022$, $C_D = 0.01$, $R_b = 0.08$ m and $\rho_a = 1.225$ kg/m^3. In Fig. 3, the top plot presents variations of thrust force with respect to blade azimuth. The red color represents the thrust force when $\|\boldsymbol{V}_{\infty_1}\| = 0$, which

is constant, meaning that the relative air flow velocity over the blade element is constant for all azimuth angles. The blue color, represents thrust force of the propeller as a function of azimuth angle when freestream velocity is nonzero, $\|\boldsymbol{V}_{\infty_1}\| = 10$ m/s.

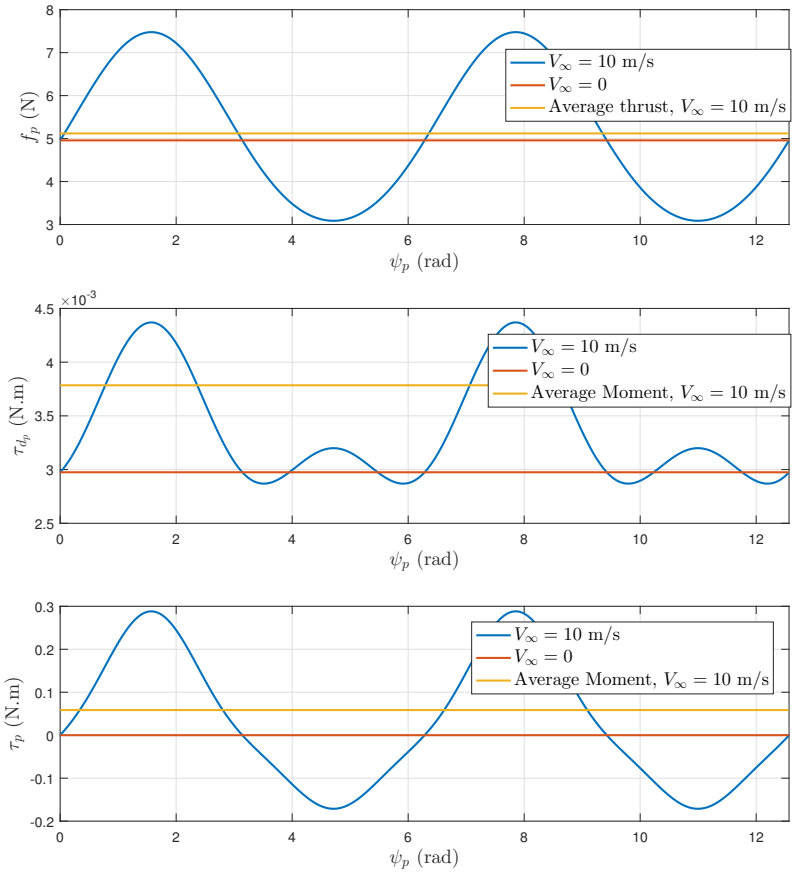

Fig. 3. Simulation results for thrust force and moments of a propeller in presence of freestream.

Comparing both scenarios, it can be seen that for nonzero freestream velocity and for $0 \leq \psi_p \leq \pi$ thrust force is increased while for $\pi \leq \psi_p \leq 2\pi$ thrust force is decreased which is due to higher relative air flow velocities on the advancing blade than that over the retreating blade. The yellow color shows the average

of thrust force of the propeller when $\|\boldsymbol{V}_{\infty_1}\| = 10$ m/s. Results show that in presence of nonzero freestream velocity the average thrust force of the propeller increases.

The middle and bottom plots in Fig. 3 present variations of the moments due to drag and freestream (τ_{d_p} and τ_p) versus azimuth angle respectively. The red color represents the moment when $\|\boldsymbol{V}_{\infty_1}\| = 0$ m/s, blue color represents variations of moment in presence of freestream velocity $\|\boldsymbol{V}_{\infty_1}\| = 10$ m/s and the yellow color represents the average moment of the propeller when $\|\boldsymbol{V}_{\infty_1}\| = 10$ m/s.

To continue investigating the effects of freestream on propeller's performance, as shown in Fig. 4, assume the freestream velocity vector, $\boldsymbol{V}_{\infty_2}$, is parallel to the angular velocity vector of the propeller, $\boldsymbol{\omega}_p$. Suppose the propeller is turning with angular velocity $\boldsymbol{\omega}_p$ as shown in Fig. 5. In absence of freestream, there will be an airflow velocity vector $r_b\boldsymbol{\omega}_p$ over each blade element as shown in green. Also, for each blade element, the angle of attack (AOA) Θ is defined as the angle between the chord of the blade element and the local airflow velocity vector $r_b\boldsymbol{\omega}_p$.

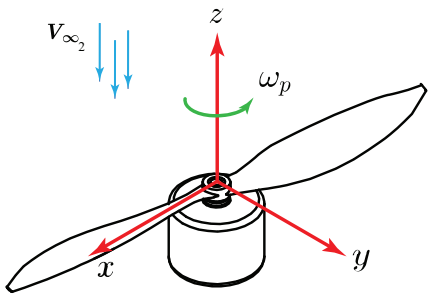

Fig. 4. Propeller in presence of freestream. The freestream velocity vector $\boldsymbol{V}_{\infty_2}$ is assumed to be parallel with the angular velocity vector of the propeller $\boldsymbol{\omega}_p$.

Now, consider an uniform freestream with velocity vector $\boldsymbol{V}_{\infty_2}$ in the positive direction of z-axis as shown in blue in Fig. 5 top. As shown, the freestream changes the direction and magnitude of the resultant airflow velocity over the blade element as shown in red in Fig. 5 top. Therefore, the new angle of attack Θ', in presence of freestream is greater than that in absence of freestream ($\Theta' \geq \Theta$).

However, if the freestream velocity vector is in the negative direction of z-axis (see Fig. 5 bottom), it changes the direction and magnitude of the resultant airflow velocity vector such that it decreases the effective angle of attack ($\Theta' \leq \Theta$).

The importance of studying AOA is because it directly affects the lift coefficient of the blade element and consequently affects the thrust force generated by the propeller. In low speed flight regimes (subsonic) and assuming small angles for AOA, the lift coefficient C_L changes almost linearly with AOA which can be

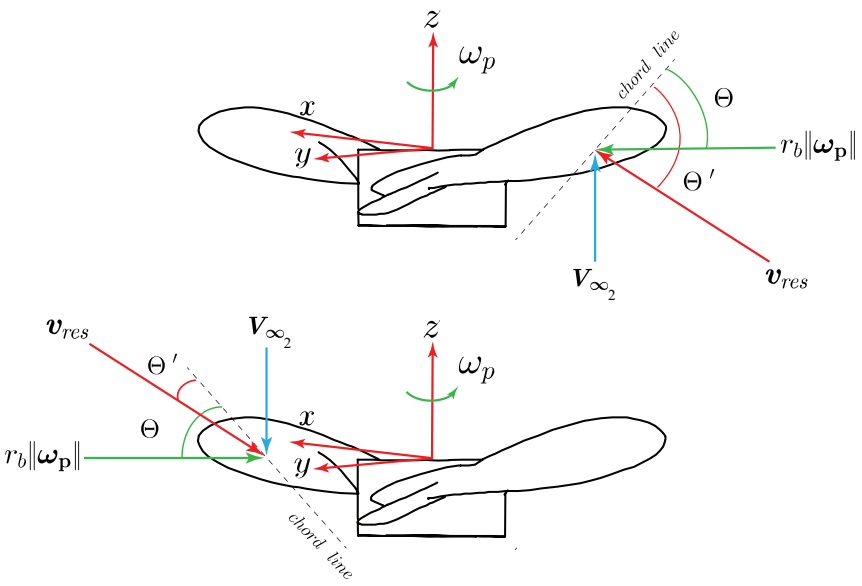

Fig. 5. Propeller in presence of freestream. The freestream velocity vector $\boldsymbol{V}_{\infty_2}$ is assumed to be parallel with $\boldsymbol{\omega}_p$. On top, $\boldsymbol{V}_{\infty_2}$ is the positive direction of z-axis and in bottom it is assumed to be in the opposite direction.

written as follows [17]:

$$\frac{\Delta C_L}{\Delta \Theta} = \sigma \tag{8}$$

where σ is a constant which is determined through experiments in wind tunnel. From (2), any increase (decrease) in C_L increases (decrease) the thrust force of the blade element. Therefore, in summary the results are as follows:

– *Any freestream with positive (negative) z-component velocity (expressed in the propeller's frame) increases (decreases) the AOA which increases (decreases) the thrust force.*

Furthermore, to formulate the changes in thrust force of the propeller, first we can write the changes in AOA of each blade element as follows:

$$\Delta\Theta = \Theta - \Theta' = \arctan \frac{\|\boldsymbol{V}_{\infty_2}\|}{\|r_b \boldsymbol{\omega}_p\|} \tag{9}$$

Finally, using (2), (8) and (9), the changes in thrust force of the propeller can be written as follows:

$$\Delta f_p = \frac{1}{4}\rho_a c \sigma R_b^2 \|\boldsymbol{V}_{\infty_2}\| \|\boldsymbol{\omega}_p\| \tag{10}$$

From (10), it can be seen that the changes in thrust force is proportional to the magnitude of the freestream velocity vector $\boldsymbol{V}_{\infty_2}$.

In summary, we presented the significance of the effects of freestream on performance of propellers. We formulated these effects as functions of propeller parameters and also the parameters of the freestream. Table 1 presents all parameters involved in the proposed propeller model. We continue this chapter by presenting mathematical modeling of two types of multi-rotor UAVs, namely quadcopters and spinners, using the proposed propeller model.

Table 1. Parameters used in modeling propeller's thrust and moments.

Parameter	Definition
$\boldsymbol{\omega}_p$	angular velocity vector of the propeller
Θ	angle of attack
C_L, C_D	lift and drag coefficients of the airfoil
$\boldsymbol{V}_\infty$	freestream velocity vector
σ	slope of C_L vs Θ curve for the airfoil
R_b	blade radius of the propeller
c	chord of the blade
r_b	distance from blade element to root of the blade
ρ_a	air density
f_p	thrust force of the propeller
τ_{d_p}	moment of the propeller due to drag
τ_p	moment of the propeller due to asymmetrical lift distribution

3 Dynamic Model of Quadcopters with Angled Thrust Vectors

This section presents mathematical modeling of quadcopters with angled thrust vectors by utilizing the proposed model of the propeller in the previous section. Literature pertinent to the mathematical modeling of quadcopters and their flight control is vast. In our derivation, we assume a full model of the gyroscopic moments and cross-coupling of angular momentum in the system. More specifically, we derive the dynamic model of quadcopters assuming that: i) the thrust vector for each rotor would make a non-zero angle with the vertical axis of the quadcopter; and ii) the center of mass (COM) of the quadcopter does not lie on the same plane where the center-of-mass of all the motors lie on (blue plane shown in Fig. 6). However, we still assume that the geometry of quadcopter fuselage is symmetric with respect to both x and y axes.

The angle between the thrust vector of each rotor and the vertical axis of the fuselage is further divided into: i) the dihedral angle; and ii) twist (i.e., lateral tilting) angle (Figs 7 and 8). We assume that the central hub of all four rotors

lie on a flat horizontal plane (blue plane in Fig. 6), called flat plane from this point on, from which the location of the COM is referenced (i.e., the COM can be either above, below, or right on this plane).

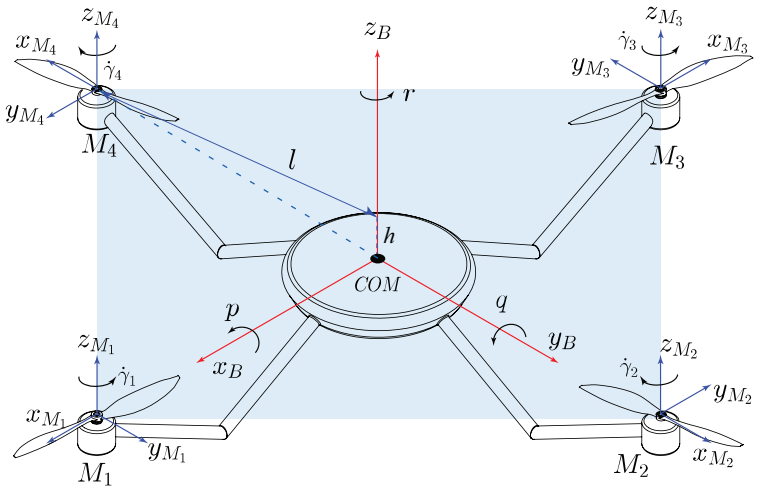

Fig. 6. Quadcopter in "+" configuration. Body frame is shown in blue and is attached to the center-of-mass of the quadcopter. A frame, shown in blue, is attached to each motor to determine orientation of the motors with respect to the body frame. All the motors are located at distance l and h from z-axis and x-y plane of the body frame respectively.

The dynamic model developed in this section has three additional terms compared to that in the flat quadcopters (this is the term used for the regular common quadcopters), as: dihedral angle β_i, twist angle α_i, and the distance between the COM and the flat plane h (please note that h could take positive and negative values, measured in z-direction of the body frame). In the flat model of quadcopters one has: $\beta_i = \alpha_i = d = 0$. We use Newton's method for deriving the dynamic model of the quadcopter and we assume a "+" configuration.

The body frame ${}^{B}O - {}^{B}x{}^{B}y{}^{B}z$ (red color in Fig. 6) is attached to the center of mass of the vehicle. Four frames named ${}^{M_i}O - {}^{M_i}x{}^{M_i}y{}^{M_i}z$ (blue color in Fig. 6) are attached to motors. Motors are turning with angular velocities $\dot{\gamma}_i$ $(i = 1, 2, ..., 4)$ about z_{M_i}-axis. Position of the vehicle is expressed in the inertial frame I. Also ${}^{B}\boldsymbol{\omega}_{p_i,I}$ indicates that $\boldsymbol{\omega}$ belongs to the i^{th} propeller with respect to an inertial frame I and is expressed in the body frame B. Finally, we represent a rotation matrix about axis A by angle θ as $\mathbf{R}_A(\theta)$.

Orientation of the body frame with respect to the inertial frame can be captured by the rotation matrix ${}^{I}\mathbf{R}_B$ from body frame to inertial frame. This rotation matrix is a function of time and its evolution in time can be obtained

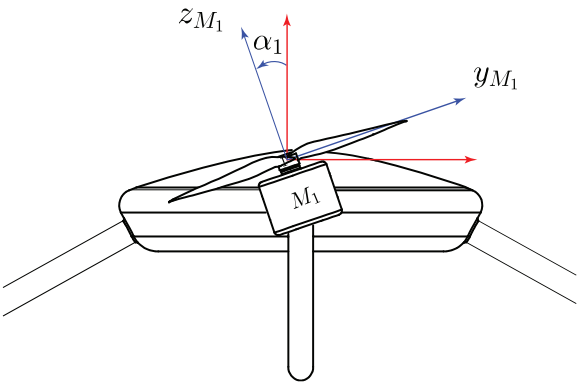

Fig. 7. Twist angle α_1 about the x-axis of the motor frame M_1.

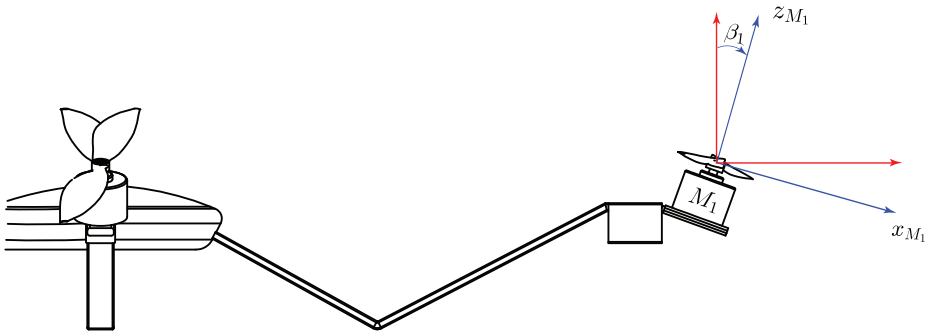

Fig. 8. Dihedral angle β_1 about the y-axis of the motor frame M_1.

as follows:

$$ {}^{I}\dot{\mathbf{R}}_{B} = {}^{I}\mathbf{R}_{B}\,\mathrm{sk}({}^{B}\boldsymbol{\omega}_{B,I}) \tag{11} $$

where $\mathrm{sk}({}^{B}\boldsymbol{\omega}_{B,I})$ is the skew-symmetric matrix of angular velocity of the body with respect to the inertial frame as expressed in the body frame ${}^{B}\boldsymbol{\omega}_{B,I} = [p, q, r]^T$.

Likewise, the orientation of each motor frame M_i can be obtained with respect to the body frame. First the position of the origin of frame M_i with respect to body frame from the origin of the body frame can be written as:

$$ {}^{B}\boldsymbol{O}_{M_i} = \mathbf{R}_{z_B}((i-1)\frac{\pi}{2}) \begin{bmatrix} l \\ 0 \\ h \end{bmatrix} , \quad (i = 1, 2, ..., 4) \tag{12} $$

Since we are using a quadcopter in "+" configuration, we assume that the motors are evenly distributed by angle $\frac{\pi}{2}$ about z_B-axis. Therefore, the transformation from frame M_i to body frame is obtained as follows:

$$ {}^{B}\mathbf{R}_{M_i} = \mathbf{R}_{z}((i-1)\frac{\pi}{2})\mathbf{R}_{y}(\beta_i)\mathbf{R}_{x}(\alpha_i) , \quad (i = 1, 2, ..., 4) \tag{13} $$

Suppose the quadcopter is consisted of several rigid bodies and it is considered to be symmetric about its axes of rotation. Because of the symmetry, the inertia tensor of the vehicle, $\mathbf{I}^B$, will be diagonal and is expressed in the body frame. We also assume that the moment of inertia of the propellers, $\mathbf{I}^p$, are very small compared to $\mathbf{I}^B$. We can neglect drag force in angular motion of the body by assuming very small angular velocities. Considering these simplifying assumptions, the rotational motion is governed by the following equation:

$$\boldsymbol{\tau} = \mathbf{I}^B \dot{\boldsymbol{\omega}}_{B,I} + \sum_{i=1}^{4} \mathbf{I}^p {}^B\dot{\boldsymbol{\omega}}_{p_i} + {}^B\boldsymbol{\omega}_{B,I} \times \left(\mathbf{I}^B \boldsymbol{\omega}_{B,I} + \sum_{i=1}^{4} \mathbf{I}^p {}^B\boldsymbol{\omega}_{p_i} \right) \tag{14}$$

where ${}^B\boldsymbol{\omega}_{p_i}$ is the angular velocity vector of the i^{th} propeller with respect to the inertial frame as expressed in the body frame which can be written as follows:

$${}^B\boldsymbol{\omega}_{p_i} = {}^B\mathbf{R}_{M_i}[0, 0, \dot{\gamma}_i^2]^T \tag{15}$$

where $\dot{\gamma}_i$ is the angular velocity of the i^{th} propeller about z-axis of frame M_i. In (14), $\boldsymbol{\tau}$ is the external moment generated by thrust forces and the reaction from propellers plus the drag of the fuselage expressed in the body frame ($\boldsymbol{\tau}_{d_B}$). Thrust force and reaction moment of each propeller as expressed in the frame M_i, can be calculated using the proposed propeller model in the previous section. The external moment $\boldsymbol{\tau}$ can be written as follows:

$$\boldsymbol{\tau} = \boldsymbol{\tau}_{d_B} + \sum_{i=1}^{4} \left({}^B\boldsymbol{O}_{M_i} \times {}^B\mathbf{R}_{M_i} {}^{M_i}\boldsymbol{f}_{p_i} + {}^B\mathbf{R}_{M_i} \left({}^{M_i}\boldsymbol{\tau}_{p_i} + {}^{M_i}\boldsymbol{\tau}_{d_{p_i}} \right) \right) \tag{16}$$

The position of the vehicle in inertial frame is shown by Cartesian coordinates $\boldsymbol{d} = [d_1, d_2, d_3]^T$. Therefore, the equation governing translational motion can be written as follows:

$$m\ddot{\boldsymbol{d}} = {}^I\mathbf{R}_B \sum_{i=1}^{4} \left({}^B\mathbf{R}_{M_i} {}^{M_i}\boldsymbol{f}_{p_i} \right) + m\boldsymbol{g} \tag{17}$$

where m is total mass of the vehicle and $\boldsymbol{g}$ is gravitational acceleration vector expressed in the inertial frame. Note that we assume small translational velocities, therefore the drag forces due to translational motion can be neglected in (17).

Although the changes in propeller's thrust force and moments in presence of freestream seem to be insignifant in quadcopters, a detailed study in [12] reveals their significant effects on stability/maneuverablity of quadcopters. According to this study, by manipulating the dihedral and twist angles, the most statically stable as well as the most maneuverable configurations for quadcopters can be found.

4 Dynamic Model of Spinning UAVs with Streamline-shape Fuselage

In this section, dynamic model of a spinning UAV including aerodynamic model of a propeller in presence of freestream velocity is presented for the first time followed by introducing two specific configurations namely, monospinner and bispinner.

Fig. 9 shows a vehicle of mass m with a streamline-shape fuselage. Two rotors are positioned at $\boldsymbol{p}_1 = (0, l_1, h_1)$ and $\boldsymbol{p}_2 = (0, l_2, h_2)$ in the y-z plane of the body frame, B, as shown in blue. The i^{th} rotor can rotate independently about the y-axis of the body frame by angle δ_i with rotations in the direction of positive y-axis resulting in positive angles. A propeller is attached to each rotor turning with angular velocity $\omega_{p_i}\boldsymbol{e}_{p_i}$ where ω_{p_i} is the magnitude of angular velocity and $\boldsymbol{e}_{p_i}$ is the unit vector determining the direction of rotation of the i^{th} propeller in the body frame. Also, the angular velocity of the fuselage with respect to the inertial frame as expressed in the body frame is represented by $\boldsymbol{\omega}_B = (p, q, r)^T$. Furthermore, it is assumed the propeller has two blades with chord c_p and radius R_p. The fuselage is to be streamline-shape, aerodynamic and similar to the propeller with four blades with chord c_B and radius R_B. It is also assumed that the chord is constant throughout the radius of the blades.

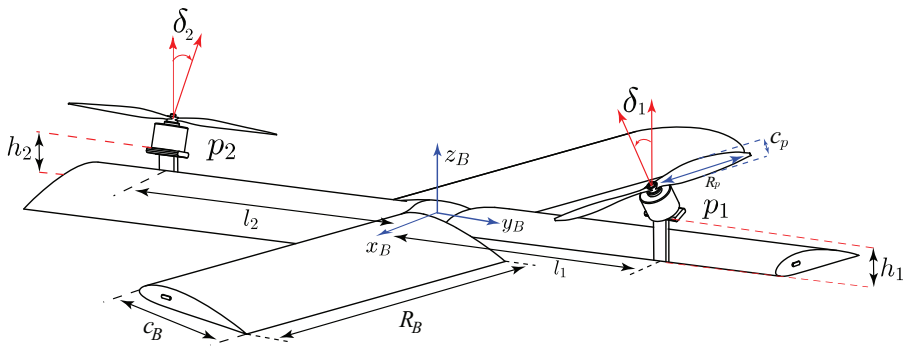

Fig. 9. A spinning UAV with two rotors and streamline-shape fuselage.

The moment of inertia matrix of the propeller is approximated by the moment of inertia of a disk as expressed in the body frame by $\mathbf{I}^p = \text{diag}(I^p_{xx}, I^p_{yy}, I^p_{zz})$. The moment of inertia matrix of the fuselage is also represented by a diagonal matrix $\mathbf{I}^B = \text{diag}(I^B_{xx}, I^B_{yy}, I^B_{zz})$. Furthermore, it is assumed that the fuselage is symmetric such that $I^B_{xx} = I^B_{yy}$. In addition, the position of the vehicle expressed in inertial frame is denoted by $\boldsymbol{d} = (d_1, d_2, d_3)$. The equations of motion can now be written as follows:

$$\boldsymbol{\tau} = \mathbf{I}^B\dot{\boldsymbol{\omega}}_B + \sum_{i=1}^{2} \mathrm{I}^p\dot{\boldsymbol{\omega}}_{p_i} + \mathrm{sk}(\boldsymbol{\omega}_B)\Big(\mathbf{I}^B\boldsymbol{\omega}_B + \sum_{i=1}^{2} \mathrm{I}^p(\boldsymbol{\omega}_{p_i} + \boldsymbol{\omega}_B)\Big) \tag{18}$$

$$\boldsymbol{\tau} = \sum_{i=1}^{2} \Big(\boldsymbol{p}_i \times \boldsymbol{f}_{p_i} \Big) + \sum_{i=1}^{2} \boldsymbol{\tau}_{d_{p_i}} + \boldsymbol{\tau}_{d_B} + \sum_{i=1}^{2} \boldsymbol{\tau}_{p_i} \tag{19}$$

$$m\ddot{\boldsymbol{d}} = {}^{I}\mathbf{R}_B \Big(\sum_{i=1}^{2} \boldsymbol{f}_{p_i} + \boldsymbol{f}_B \Big) + m\boldsymbol{g} \tag{20}$$

In the right hand side of (18), the first two terms represent the moments due to angular accelerations of the fuselage and propellers. The third term represents cross-coupling of angular momentum due to rotation of the fuselage and propellers and $\mathrm{sk}(\boldsymbol{\omega}_B)$ represents the skew-symmetric matrix of the angular velocity vector of the fuselage. In the right hand side of (19), the first term represents the moment due to propeller's thrust force about the center of mass of the vehicle, the second term represents the sum of reaction moments of the propellers, the third term is the moment due to drag of the fuselage and the last term is the sum of moments due to asymmetrical lift distribution over the advancing and retreating blades of the propellers.

In (20), $\boldsymbol{f}_B$ represents thrust force generated by the streamline-shape fuselage, $\boldsymbol{g}$ is the gravitational acceleration and ${}^{I}\mathbf{R}_B$ is the rotation matrix from body frame to inertial frame. Since the fuselage is turning with yaw rate r about the z-axis of the body frame, it generates a thrust force $\boldsymbol{f}_B$ along with a moment $\boldsymbol{\tau}_{d_B}$ due to its aerodynamic drag, in the direction of z-axis of the body frame. These can be calculated using *Blade Element Theory* as follows:

$$\boldsymbol{f}_B = \frac{1}{3}\rho_a c_B C_{L_B} R_B^3 r^2 \, \boldsymbol{e}_{\boldsymbol{f}_B} \tag{21}$$

$$\boldsymbol{\tau}_{d_B} = \frac{1}{4}\rho_a c_B C_{D_B} R_B^4 r^2 \, \boldsymbol{e}_{\boldsymbol{\tau}_{d_B}} \tag{22}$$

where ρ_a is the air density and C_{L_B} and C_{D_B} are lift and drag coefficients of the fuselage respectively. Also, $\boldsymbol{e}_{\boldsymbol{f}_B}$ and $\boldsymbol{e}_{\boldsymbol{\tau}_{d_B}}$ represent unit vectors showing the direction of thrust force and moment of the fuselage respectively. In both propellers and the fuselage, we assume the lift and drag coefficients, C_L and C_D are functions of angle of attack Θ as follows:

$$C_L = f_L(\Theta) \qquad C_D = f_D(\Theta) \tag{23}$$

From experimental results in [18], the functions f_L and f_D used in (23) can be approximated for small angle of attacks ($-10^\circ \leq \Theta \leq 10^\circ$).

4.1 Effects of Freestream in Spinning UAVs

In this section, based on the propeller model proposed in this chapter, we derive equations to determine the effective angle of attack, thrust force and moments of the propellers in a spinning UAV.

Suppose a propeller is turning with angular velocity vector $\boldsymbol{\omega}_p$ as shown in Fig. 10. The rotor is positioned at distance l from COM of the vehicle and is tilted by angle δ about the y-axis of the body frame and the fuselage is spinning

at yaw rate r about the z-axis of the body frame as shown in Fig. 10. As the vehicle is spinning, the propeller experiences an uniform freestream expressed in the body frame as:

$$^{B}\boldsymbol{V}_{\infty} = (rl, 0, 0)^{T} \tag{24}$$

Because of the tilting angle δ, this freestream will have vertical and horizontal components in the propeller's plane. According to *Blade Element Theory*, the vertical component changes the effective angle of attack of the blades as follows:

$$\Theta_{eff} = \theta + \arctan \frac{rl \sin \delta}{|R_p(\|\boldsymbol{\omega}_p\| + r \cos \delta)|} \tag{25}$$

where θ is the pitch angle of the blade, R_p is the blade radius and $(\|\boldsymbol{\omega}_p\| + r \cos \delta)$ is the resultant angular velocity of the propeller with respect to the inertial frame. Equation (25) indicates that depending on the sign of tilting angle and the yaw rate, the effective angle of attack could be either increased or decreased.

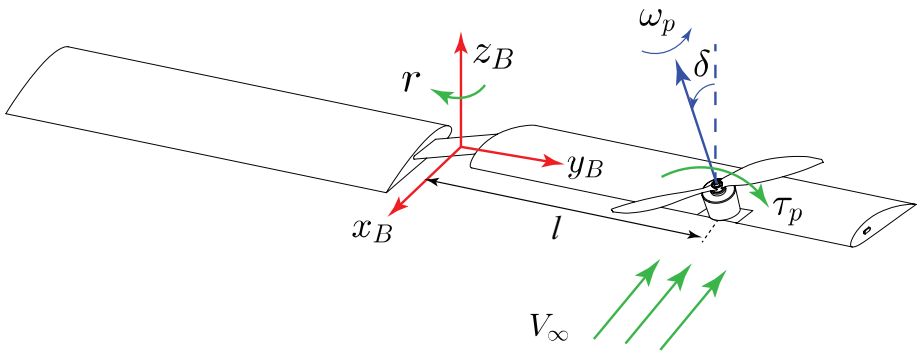

Fig. 10. Effects of freestream on propeller's performance in a spinning UAV.

We have shown that the horizontal component of freestream velocity (perpendicular to that of the propeller) changes the local airflow velocity over each blade element. Also, the vertical component of freestream velocity (parallel to that of the propeller) changes the effective angle of attack of the blade elements. Therefore, considering these changes and according to equations (5), (6) and (7), thrust force and the moments generated by the propeller can be rewritten as follows:

$$\boldsymbol{f}_p = \rho_a c_p C_{L_p} \left(\frac{R_p^3 \|\boldsymbol{\omega}_p\|^2}{3} + \frac{R_p^3 r^2 \cos^2 \delta}{3} + \frac{R_p r^2 l^2 \cos^2 \delta}{2} + \frac{2R_p^3 r \|\boldsymbol{\omega}_p\| \cos \delta}{3} \right) \boldsymbol{e}_{\boldsymbol{f}_p} \tag{26}$$

$$\boldsymbol{\tau}_{d_p} = \rho_a c_p C_{D_p} \left(\frac{R_p^4 \|\boldsymbol{\omega}_p\|^2}{4} + \frac{R_p^4 r^2 \cos^2 \delta}{4} + \frac{R_p^2 r^2 l^2 \cos^2 \delta}{2} + \frac{R_p^4 r \|\boldsymbol{\omega}_p\| \cos \delta}{2} \right) \boldsymbol{e}_{\boldsymbol{\tau}_{d_p}} \tag{27}$$

$$\boldsymbol{\tau}_p = \rho_a c_p C_{L_p} \left(\frac{R_p^3 \|\boldsymbol{\omega}_p\| r l \cos\delta + R_p^3 r^2 l \cos^2\delta}{3} \right) \boldsymbol{e}_{\boldsymbol{\tau}_p} \tag{28}$$

where $\boldsymbol{e}_{\boldsymbol{f}_p}$, $\boldsymbol{e}_{\boldsymbol{\tau}_{d_p}}$ and $\boldsymbol{e}_{\boldsymbol{\tau}_p}$ are unit vectors expressed in the body frame to determine the directions of propeller's thrust force, reaction moment and the moment due to asymmetrical lift distribution respectively.

Finally, by adding the following constraints to the system, two specific configurations namely monospinner and bispinner, are introduced. The first configuration is achieved when $l_1 = l_2 = l$, $\delta_1 = \delta_2 = \delta$ and h_2 is slightly larger or smaller than h_1 such that the second rotor can be positioned either above or below the first rotor (e.g., $h_2 = 1.1h_1 = h$) . This configuration is also known as monospinner since the two rotors could be replaced by a single rotor which yields to the simplest possible configuration for a multi-rotor flying vehicle. The second configuration is defined such that $l_2 = -l_1 = l$, $\delta_2 = -\delta_1 = \delta$ and $h_1 = h_2 = h$, also known as bispinner which provides more stability and improved controllability compared to the monospinner.

5 Conclusion

A complete mathematical model for thrust force and moments generated by a propeller in presence of an uniform freestream is presented. Using simulation results, it is shown that nonzero freestream velocity has siginifcant effects on both thrust force and moments of the propeller. The proposed model is used to derive complete equations of motion of two types of multi-rotor UAVs. First, equations of motion of a quadcopter with angled thrust vector is presented followed by sine remarks on applications and effects of the proposed propeller model on stability and maneuverability of quadcopters. Second, a new type of spinning UAVs with streamline-shape fuselage is introduced where the proposed propeller model is paramount in deriving its equations of motion. The proposed mathematical models can be used in testing and evaluating sophisticated control strategies as well as being used in designing more accurate simulators for multi-rotor UAVs.

References

1. Thomas, J., Polin, J., Sreenath, K., , Kumar, V.: Avian-inspired grasping for quadcopter micro uavs. Bioinspiration & Biomimetics 9, 25010–25019 (2014)
2. Rasmussen, J., Nielsen, J., Garcia-Ruiz, F., Christensen, S., Streibig, J.C.: Potential uses of small unmanned aircraft systems (uas) in weed research. Weed Research 4(53), 242–248 (2013)
3. Horandel, J.R., Buitink, S., Corstanje, A., Enriquez, J.E., , Falcke, H.: The lofar radio telescope as a cosmic ray detector. In: International Cosmic Ray Conference (2013)
4. Luque-Vega, L.F., Castillo-Toledo, B., Loukianov, A., Gonzalez-Jimenez, L.E.: Power line inspection via an unmanned aerial system based on the quadrotor helicopter. In: MELECON 2014 - 17th IEEE Mediterranean Electrotechnical Conference. pp. 393–397 (April 2014)

5. Bouabdallah, S., Siegwart, R.: Full control of a quadcopter. In: 2007 IEEE/RSJ International Conference on Intelligent Robots and Systems. pp. 153–158 (2007)
6. Hua, M.D., Hamel, T., Morin, P., Samson, C.: A control approach for thrust-propelled underactuated vehicles and its application to vtol drones. IEEE Transactions on Automatic Control 54(8), 1837–1853 (Aug 2009)
7. Mahony, R., Kumar, V., Corke, P.: Multirotor aerial vehicles: Modeling, estimation, and control of quadrotor. IEEE Robotics Automation Magazine 19(3), 20–32 (Sept 2012)
8. Hedayatpour, M., Mehrandezh, M., Janabi-Sharifi, F.: Revised propeller dynamics and energy-optimal hovering in a monospinner. In: The 4th International Conference of Control, Dynamic Systems, and Robotics. pp. 1–8 (August 2017)
9. Amir, M.Y., Abbass, V.: Modeling of quadrotor helicopter dynamics. In: International Conference on Smart Manufacturing Application. pp. 100–105 (2008)
10. Mellinger, D., Michael, N., Kumar, V.: Trajectory generation and control for precise aggressive maneuvers with quadrotors. The International Journal of Robotics Research 31(5), 664–674 (2012)
11. Wang, J., Bierling, T., Achtelik, M., Hocht, L., Holzapfel, F., Zhao, W., Hiong, G.: Attitude free position control of a quadcopter using dynamic inversion. In: AIAA Infotech@ Aerospace. pp. 29–31 (2011)
12. Hedayatpour, M., Mehrandezh, M., Janabi-Sharifi, F.: A unified approach to configuration-based dynamic analysis of quadcopters for optimal stability. In: 2017 IEEE/RSJ International Conference on Intelligent Robots and Systems (IROS). pp. 5116–5121 (Sept 2017)
13. Muller, M., Lupashin, S., D'Andrea, R.: Tquadrocopter ball juggling. In: 2017 IEEE/RSJ International Conference on Intelligent Robots and Systems (IROS). pp. 5113–5120 (2011)
14. Mueller, M.W., D'Andrea, R.: Relaxed hover solutions for multicopters: application to algorithmic redundancy and novel vehicles. International Journal of Robotics Research 35(8), 873–889 (2015)
15. Mueller, M.W., D'Andrea, R.: Stability and control of a quadrocopter despite the complete loss of one, two, or three propellers. In: 2014 IEEE International Conference on Robotics and Automation (ICRA). p. 4552 (2014)
16. Hehn, M., D'Andrea, R.: Quadrocopter trajectory generation and control. In: 18th IFAC World Congress, Milano. pp. 1485–1491 (2011)
17. Anderson, J.D.: Fundamentals of Aerodynamics. McGraw Hill Higher Education, United States, 5 edn. (2016)
18. Experimental data for naca airfoils. http://m-selig.ae.illinois.edu/ads/coord{_}database.html

Author Index